



ELSEVIER

Contents lists available at [SciVerse ScienceDirect](http://www.sciencedirect.com)

Comptes Rendus Physique

www.sciencedirect.com

Physics in High Magnetic Fields / Physique en champ magnétique intense

From quantum oscillations to charge order in high- T_c copper oxides in high magnetic fields*Des oscillations quantiques à un ordre de charge dans des cuprates supraconducteurs à haute- T_c en champ magnétique intense*Baptiste Vignolle^a, David Vignolles^a, Marc-Henri Julien^b, Cyril Proust^{a,*}^a Laboratoire national des champs magnétiques intenses (CNRS-INSA-UJF-UPS), 31400 Toulouse, France^b Laboratoire national des champs magnétiques intenses (CNRS-INSA-UJF-UPS), 38042 Grenoble, France

ARTICLE INFO

Article history:

Available online 16 January 2013

Keywords:

High T_c cuprate superconductor
Quantum oscillation
Nuclear magnetic resonance
Magnetotransport

Mots-clés:

Cuprate supraconducteur haute- T_c
Oscillation quantique
Résonance magnétique nucléaire
Transport sous champ magnétique

ABSTRACT

This article constitutes an update made of numerous elements from an article by Vignolle et al. [C. R. Phys. 12 (2011) 446] published in the issue of C. R. Physique dedicated to superconductivity. By including this article to the present issue on physics in high magnetic field, we have aimed, in agreement with the editorial board of the review, offering a complete issue and also reporting on the last developments in the study of superconductors in high field.

We review how experiments in very high magnetic fields over the last five years have given a new twist to the understanding of the normal state of hole-doped cuprate superconductors. The discovery of quantum oscillations in underdoped $\text{YBa}_2\text{Cu}_3\text{O}_y$ and overdoped $\text{Tl}_2\text{Ba}_2\text{CuO}_{6+\delta}$ has proven the existence of a Fermi surface across the whole phase diagram, which had been a controversial issue for more than twenty years. However, the striking difference in oscillation frequency for the two compounds has revealed a very different Fermi surface topology. The observation of negative Hall and Seebeck coefficients in the underdoped materials has shown that the large hole-like Fermi surface of overdoped materials undergoes a reconstruction in the high field and low temperature limits for which quantum oscillation can be observed. This has been interpreted as evidence for a translational symmetry breaking due to some form of electronic (spin, charge, or orbital current) order. The angular dependence of the quantum oscillations has constrained the source of the Fermi-surface reconstruction to something other than a spin-density wave with moments perpendicular to the field. Finally, nuclear magnetic resonance studies have revealed that it is actually charge order, without spin order, which is induced in the copper oxide planes as soon as superconductivity is sufficiently weakened by the magnetic field. The results suggest that there is a generic competition between superconductivity and a charge-density-wave instability in high T_c cuprates.

© 2012 Académie des sciences. Published by Elsevier Masson SAS. All rights reserved.

R É S U M É

Cet article constitue une mise à jour reprenant beaucoup d'éléments d'un article de Vignolle et al. [C. R. Phys. 12 (2011) 446] publié dans un dossier des C. R. Physique dédié à la supraconductivité. En incluant cet article dans le présent dossier sur la physique en champ magnétique intense nous avons souhaité, en accord avec le Collège éditorial de la

* Corresponding author.

E-mail address: Cyril.Proust@lncmi.cnrs.fr (C. Proust).

revue, offrir un dossier complet mais aussi rendre compte des derniers développements dans l'étude des supraconducteurs en fort champ.

Nous discutons comment, au cours des dernières années, certaines expériences sous champ magnétique intense ont donné une nouvelle tournure à la compréhension de l'état normal des cuprates supraconducteurs dopés en trous. La découverte des oscillations quantiques dans $\text{YBa}_2\text{Cu}_3\text{O}_y$ sous-dopé et $\text{Tl}_2\text{Ba}_2\text{CuO}_{6+\delta}$ sur-dopé a démontré l'existence d'une surface de Fermi à travers le diagramme de phase, ce qui était une question controversée depuis plus de vingt ans. Cependant, la différence de fréquence d'oscillation pour les deux composés a révélé une topologie très différente de leur surface de Fermi. De surcroît, l'observation des coefficients Hall et Seebeck négatifs dans les matériaux sous-dopé a montré que la grande surface de Fermi de trou des matériaux sur-dopés a subi une reconstruction dans la limite fort champ magnétique et basse température où les oscillations quantiques ont été observées. Cela a été interprété comme l'existence d'une brisure de symétrie due à un ordre électronique (de spin, de charge, ou de courants orbitaux). La dépendance angulaire des oscillations quantiques a permis de conclure que la reconstruction de la surface de Fermi n'était pas la conséquence d'une onde de densité de spin avec des moments perpendiculaires au champ. Enfin, des mesures de résonance magnétique nucléaire ont révélé que c'est en fait un ordre de charge, sans ordre de spin, qui est induit dans les plans d'oxyde de cuivre dès que la supraconductivité est suffisamment affaiblie par le champ magnétique. Ces résultats suggèrent qu'il existe une compétition générique entre la supraconductivité et une onde de densité de charge dans les cuprates supraconducteurs.

© 2012 Académie des sciences. Published by Elsevier Masson SAS. All rights reserved.

1. Introduction

The generic phase diagram of hole-doped cuprates shown in Fig. 1 shows that high temperature superconductivity is sandwiched between an insulating and a Fermi liquid phase. At zero doping, band structure calculations predict the conducting band to be half-filled and therefore the system to be metallic. However, the strong electron–electron correlations (strong on-site Coulomb repulsion) impedes electrons to hop from one atom to another. The resulting ground state is a Mott insulator, which adopts an antiferromagnetic (AF) configuration for the Cu spin 1/2. The AF phase is rapidly destabilized when carriers are added in the CuO_2 planes and the Néel temperature T_N vanishes at $p \approx 0.05$ for $\text{YBa}_2\text{Cu}_3\text{O}_y$ where the superconducting dome emerges and extends to $p \approx 0.31$ (for overdoped $\text{Tl}_2\text{Ba}_2\text{CuO}_{6+\delta}$). The optimal doping corresponds to $p \approx 0.16$ where the superconducting transition T_c is maximal. The underdoped (overdoped) regime corresponds to the left (right) part of the dome.

On the strongly overdoped side, the electronic properties can be understood within the framework of the generalized Fermi-liquid (FL) theory, the standard theory of electrons in solids. One robust signature of an FL is the observation of the Wiedemann–Franz law in overdoped $\text{Tl}_2\text{Ba}_2\text{CuO}_{6+\delta}$ [1] which demonstrates that the fermions which carry heat also carry a charge e and are therefore indistinguishable from standard Landau quasiparticles. Another strong indication of FL behaviour comes from transport measurements in heavily overdoped (non-superconducting) $\text{La}_{2-x}\text{Sr}_x\text{CuO}_4$ which shows that both ρ_{ab} and ρ_c exhibit strictly T^2 behaviour below 50 K [2]. However, as the overdoped compound becomes superconducting, an additional T-linear component of the resistivity appears as seen in resistivity [1,3,4] and angular magneto-resistance oscillation (AMRO) [5] measurements on $\text{Tl}_2\text{Ba}_2\text{CuO}_{6+\delta}$ and in high-field magneto-transport measurements in the normal state of overdoped $\text{La}_{1.6-x}\text{Nd}_{0.4}\text{Sr}_x\text{CuO}_4$ [6] and $\text{La}_{2-x}\text{Sr}_x\text{CuO}_4$ [7].

The underdoped side of the phase diagram is characterized by the presence of the mysterious *pseudogap* phase. The first evidence of the pseudogap phase came from nuclear magnetic resonance (NMR) measurements back in 1989 [8–10]. Later, angle-resolved photoemission spectroscopy (ARPES) measurements in underdoped $\text{Bi}_2\text{Sr}_2\text{CaCu}_2\text{O}_{8+\delta}$ close to the anti-nodal directions have revealed that the quasiparticle peak disappears above T_c and that there is an energy gap above T_c which persists up to T^* [11]. This gap is strongly anisotropic since it appears only at the anti-nodal region of the Fermi surface (FS). The d -wave node below T_c becomes a gapless arc above T_c which expands with increasing temperature to form the full FS at T^* . The similarity between the superconducting gap and the pseudogap might suggest that the latter is a precursor of the superconducting gap.

An alternative scenario for the pseudogap phase assumes that T^* marks the onset of an ordered phase. Several experiments suggest that T^* marks the onset of a phase with broken symmetry: using polarized elastic neutron diffraction, a novel AF order at $Q = 0$ has been identified in underdoped $\text{YBa}_2\text{Cu}_3\text{O}_y$ [12], in underdoped $\text{HgBa}_2\text{CuO}_{4+\delta}$ [13], and in underdoped $\text{Bi}_2\text{Sr}_2\text{CaCu}_2\text{O}_{8+\delta}$ [14]. Polar Kerr effect measurements in underdoped $\text{YBa}_2\text{Cu}_3\text{O}_y$ found also evidence for broken symmetry near the pseudogap temperature [15]. Recently, resonant ultrasound measurements have detected an anomaly in the elastic constant at T^* , revealing a phase transition at the pseudogap boundary [16]. Finally, Nernst effect measurements in underdoped $\text{YBa}_2\text{Cu}_3\text{O}_y$ report the observation of a large in-plane anisotropy of the Nernst coefficient that sets in at T^* [17] and scanning tunnelling spectroscopy measurements in the pseudogap phase in underdoped $\text{Bi}_2\text{Sr}_2\text{CaCu}_2\text{O}_{8+\delta}$ find

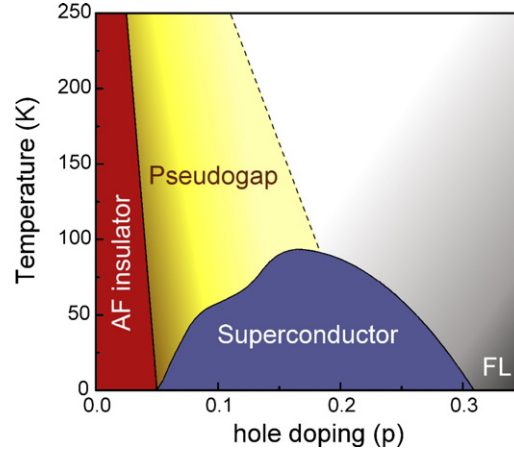


Fig. 1. Generic temperature–doping phase diagram of high temperature cuprate superconductors. The parent compound is an antiferromagnetic Mott insulator. The dotted line is a crossover which marks the appearance of the pseudogap phase. At high doping, a generalized Fermi liquid behaviour is recovered.

evidence for electronic nematicity [18], suggesting that the pseudogap phase is an electronic state that breaks four-fold rotational symmetry.

There is still no consensus as to whether the pseudogap is a precursor to or distinct from the superconducting phase [19]. In most descriptions of the doped Mott insulator, such as the “resonating valence bond” (RVB) [20] or the pre-formed pair scenario [21], the pseudogap phase corresponds to a phase with formation of either spin singlets or phase-incoherent Cooper pairs. The Fermi surface consists of 4 nodal hole pockets, with one side of each pocket having a quasiparticle residue much smaller than the other one, leading to Fermi arcs. In other classes of scenarios such as spin density wave order [22,23], stripe order [24,25], d -density wave order [26] or marginal Fermi liquid (MFL) [27], the pseudogap is not related to superconductivity but rather competes with it. Except for the MFL scenario, all these scenarios involve a Fermi surface reconstruction where the resulting FS consists of electron (and hole) sheets.

2. Magnetic quantum oscillations and NMR measurements in high field at the LNCMI

2.1. Quantum oscillations

2.1.1. Theoretical background

In the presence of a magnetic field, the energy levels of electrons are quantized into Landau levels. A full quantum mechanic treatment leads to the three-dimensional (3D) electronic dispersion for free electrons: $\varepsilon_n(k_z) = (n + \frac{1}{2})\hbar\omega_c + \frac{\hbar^2 k_z^2}{2m}$. The Landau levels are separated by the energy $\hbar\omega_c = \hbar eB/m^*$, which increases as the field increases. As the field is swept, there is a reorganization of the electronic states: each time a Landau level crosses the Fermi energy, there is a singularity in the density of states which gives rise to the oscillation of many physical properties [28]. The oscillation of the magnetization is called de Haas–van Alphen effect [29] (dHvA) and the oscillation of the resistivity is called Shubnikov–de Haas effect [30] (SdH) in tribute to the scientists who discovered these effects in elemental Bismuth in 1930. The dHvA and SdH effects are described by the Lifshitz–Kosevich (LK) theory [31]. The oscillatory part of the magnetoconductivity for a general 3D case is given by:

$$\frac{\Delta\sigma}{\sigma} \propto \sum_i A_i^0 B^{\frac{1}{2}} \sum_{p=1}^{\infty} R_T R_D R_S \cos\left(2\pi p \left[\frac{F_i}{B} - \gamma_i\right] \pm \frac{\pi}{4}\right) \quad (1)$$

The frequency F_i of the oscillation is proportional to the extremal area A_i of the FS (sum over i Fermi surfaces): $F_i = \frac{\hbar}{2\pi e} A_i$. The index p corresponds to the sum over the harmonics. γ_i is a phase factor and R_T , R_D and R_S are the thermal, impurity and spin damping factors respectively.

When the amplitude of the oscillations is small in comparison to the background, the LK formula can be applied to the oscillatory part of the magnetoresistance: $\frac{\Delta\sigma}{\sigma} \approx \frac{\Delta\rho}{\rho}$. When the amplitude of the oscillations becomes comparable to the background, then one has to work on the oscillatory part of the conductivity. Dividing the oscillatory part by the background and applying the LK formula for large amplitude oscillations would generally lead to the appearance of harmonics in the signal.

In order to observe quantum oscillations, it is necessary that the distance between Landau levels is greater than the thermal broadening, e.g. $\hbar\omega_c > k_B T$. These measurements are therefore performed at low temperature (below 10 K in the case of the cuprates). The damping factor

$$R_T = \frac{\alpha T m_i^* / B}{\sinh(\alpha T m_i^* / B)} = \frac{X}{\sinh(X)}$$

with $\alpha = 2\pi^2 m^* k_B / e \hbar$ takes into account finite temperature effects due to the broadening of the Fermi function. It allows the effective mass m^* to be deduced from the temperature dependence of the amplitude of the oscillations. m^* is the thermodynamic effective mass which includes electron–electron and electron–phonon interactions and can be compared to the one deduced from the Sommerfeld coefficient of the specific heat.

Another requirement to observe quantum oscillations is that the broadening of the Landau levels due to impurity scattering should be less than the distance between the Landau levels, e.g. $\hbar\omega_c > \hbar/\tau$ leading to $\omega_c \tau > 1$. The damping factor

$$R_D = \exp\left(-\pi \sqrt{\frac{2\hbar F_0}{e}} \frac{1}{\ell B}\right)$$

is called the Dingle factor, where ℓ is the low temperature mean free path that can be deduced from the field dependence of the amplitude of the oscillations. This term imposes the necessity to work on high quality single crystals. Due to the stronger effect of small angle scattering on the dephasing of the quantum oscillations, ℓ extracted from quantum oscillations is usually smaller than the mean free path deduced from transport measurements [32].

Finally, the damping factor

$$R_S = \cos\left(\frac{\pi g m_s}{2m_0}\right)$$

takes into account the spin splitting due to Zeeman effect. The effective mass which enters this expression is usually not the same as m^* . While the effective mass m^* (appearing in R_T) is renormalized by both electron–electron and electron–phonon interactions, m_s the ‘spin’ mass (entering in R_S) only includes electron–electron interactions: $m^* = (1 + \lambda_{\text{phonon}})m_s$ [33].

In the case of a quasi-two-dimensional (Q2D) metal, the warping of the FS manifests itself as a frequency-splitting corresponding to neck and belly frequencies, associated with the minimum and maximum cross-sections of the FS. The oscillatory part of the magnetoresistivity of the fundamental component of oscillation becomes:

$$\frac{\Delta\rho}{\rho} \propto A_0 R_T R_D R_S J_0 \left[2\pi \frac{\Delta F}{B \cos\theta} J_0(k_F c \tan\theta) \right] \cos \left[2\pi \left(\frac{F}{B \cos\theta} - \gamma \right) \right] \quad (2)$$

F is the frequency corresponding to the average area of a cylinder, ΔF is the splitting corresponding to the warping of the cylinder described by the Bessel function J_0 , k_F is the average radius of the cylinder, c is the c -axis lattice parameter, θ is the angle between the field and the c -axis, γ is a phase factor. R_T , R_D , and R_S are the damping factors discussed previously. Instead of treating the electron effective mass, the amplitude, the phase of the oscillations, and the Dingle temperature separately for the neck and belly orbits, only one value of each of these parameters is required to describe a single FS, reducing the number of fitting parameters.

2.1.2. Experimental techniques

Transport measurements up to 60 and 70 T are routinely performed at the LNCMI in Toulouse in conventional pulsed resistive magnets driven by a 24 kV, 14 MJ capacitor bank [34]. A new coil-in coil-ex magnet has recently been developed, producing 80 T with 12 ms available above 70 T, enabling high signal over noise experiments to be performed [35]. Variable temperatures are obtained using a standard ^4He cryostat for T varying from 1.5 K to 300 K and using a dilution fridge with a plastic mixing chamber for temperatures below 1.5 K. For in-plane transport measurements, longitudinal (R_{xx}) and transverse (R_{xy}) resistances are obtained from the voltage difference measured diagonally on either side of the sample width, for a field parallel (up) and anti-parallel (down) to the c -axis. Electrical contacts to the sample were made by evaporating gold pads. For longitudinal c -axis transport ($I \parallel B \parallel c$), large current pads and small voltage pads were mounted across the top and bottom so as to short out any in-plane current. A current excitation of 5 to 10 mA at 60 kHz was used. Typical dimensions of the samples are ($1 \times 1 \times 0.05 \text{ mm}^3$). We systematically checked that data collected during the rise and the fall of the field pulse are in perfect agreement, excluding any heating due to eddy currents.

2.2. Experimental techniques: NMR measurements

The NMR experiments above 17 Tesla were performed in two resistive magnets at the LNCMI-Grenoble. The maximum field of the M9 magnet is 35 T in a 34 mm bore with a homogeneity $\Delta B/B = 700 \times 10^{-6}$ over a 1 cm^3 sphere (radius 6.2 mm). M10 provides up to 30 T in a 50 mm bore and with $\Delta B/B = 860 \times 10^{-6}$. Given the small sample size of maximum $2 \times 2 \times 0.2 \text{ mm}^3$, the relevant homogeneity is actually even better (100 ppm over 5 mm) so that the broad Cu NMR spectra were not affected by the magnet homogeneity. They were also not affected by the time fluctuations of the field which are of the order of $\delta B_{\text{max}}(t)/B = \pm 10^{-5}$. The ^{27}Al NMR signal from a 0.8 μm thick aluminium foil (99.1% purity) was used to calibrate both the value of the external field and the NMR intensities. Standard spin-echo techniques were used with a home-built heterodyne spectrometer. Spectra were obtained at fixed magnetic fields by combining Fourier transforms of the spin-echo signal recorded for regularly-spaced frequency values.

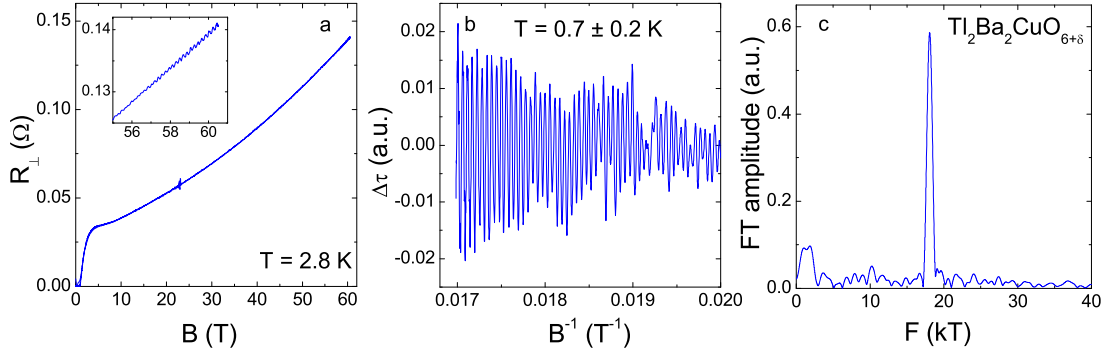


Fig. 2. (a) Magnetic field dependence of the interlayer resistance of overdoped $\text{Tl}_2\text{Ba}_2\text{CuO}_{6+\delta}$ ($T_c = 10$ K) at $T = 2.8$ K (raw data). The inset is a zoom on the high field part where quantum oscillations are seen for $B > 58$ T. (b) Oscillatory part of the torque data plotted as a function of $1/B$. (c) Fourier transform of the signal presented in (b), showing a single peak at about $F = 18100$ T (from [39]).

3. Quantum oscillations in overdoped $\text{Tl}_2\text{Ba}_2\text{CuO}_{6+\delta}$

First experimental clues for the existence of an FS in overdoped $\text{Tl}_2\text{Ba}_2\text{CuO}_{6+\delta}$ came from AMRO [36] and ARPES [37] experiments. Both probes have suggested the existence of an FS in agreement with band structure calculations [38], e.g. a large Q2D warped cylinder which represents $\sim 65\%$ of the first Brillouin zone. Nevertheless AMRO is a semi-classical probe of the underlying FS which cannot directly conclude about the coherent nature of quasiparticles and the peak of quasiparticles measured by ARPES is too broad (100 meV) to be ascribed to coherent quasiparticles. Quantum oscillations are the most sensitive probe of the FS of a metal and demonstrate that well defined quasiparticles are the low energy excitations of the system. They have long been searched for in overdoped cuprates, but have only been detected in 2008.

Quantum oscillations measurements in overdoped $\text{Tl}_2\text{Ba}_2\text{CuO}_{6+\delta}$ were performed by means of longitudinal c -axis magnetoresistance as well as torque measurements [39]. Single crystals of $\text{Tl}_2\text{Ba}_2\text{CuO}_{6+\delta}$ with $T_c \approx 10$ K have been chosen for their high crystalline quality, with a mean free path estimated from zero field transport measurements to be of the order of 100 nm [3]. Fig. 2a shows the interlayer magnetoresistance up to 60 T. Above the superconducting transition, a strong magnetoresistance develops and quantum oscillations with small amplitude emerge above the noise level from 58 T in the magnetoresistance measurements (see inset of Fig. 2a). Fig. 2b displays the oscillatory part of the torque plotted versus $1/B$. The observation of oscillations, periodic in $1/B$, in both the magnetization and the resistivity, at fields well above the upper critical field, confirms these as quantum oscillations. The Fourier transform yields the power spectrum displayed in Fig. 2c which consists in a single sharp peak at a frequency of 18100 ± 50 T. The frequency of oscillation can be related to the extremal area of the FS perpendicular to the applied magnetic field via the Onsager relation, leading to an FS cross section $A_F = 172.8 \pm 0.5 \text{ nm}^{-2}$. Assuming a cylindrical FS, the corresponding Fermi wavevector $k_F = 7.42 \pm 0.05 \text{ nm}^{-1}$ is in excellent agreement with the values deduced from AMRO ($k_F = 7.35 \pm 0.1 \text{ nm}^{-1}$) [36] and ARPES ($7.28 \pm 0.2 \text{ nm}^{-1}$) [37] at similar doping level. The Luttinger sum rule states that at 2D the density of carriers $n = 2A_F/(2\pi)^2$, that is $n = F/\phi_0$ where $\phi_0 = h/2e$ is the flux quantum. The measured frequency corresponds to a carrier density $n = 1.3 = 1 + p$ with 1 hole corresponding to the half-filled band, and p hole added by hole doping. This agrees nicely with the Hall number $n_H = 1.3$ obtained at low temperature [3].

Subsequent angular dependence of quantum oscillations in two samples at different doping level ($T_c = 10$ K and 26 K) have been performed in static fields up to 45 T at the NHMFL [40]. The frequency reported for the $T_c = 10$ K sample is in excellent agreement with the one reported in pulsed field (18100 T). The frequency of oscillations for the $T_c = 26$ K sample is 17630 T, corresponding to a carrier density $n = 1.27 = 1 + p$.

The effective mass m^* of the quasiparticles can be deduced from the temperature dependence of the quantum oscillations amplitude. Within the experimental resolution, this evolution is found to follow the Lifshitz–Kosevich formalism. The deduced effective mass measured in pulsed field $m^* = (4.1 \pm 1)m_0$, where m_0 is the free electron mass, indicates that strong electronic correlations still persist at this doping level (DFT calculations predict that the bare band mass is $1.7m_0$ at this doping level) [41]. The lower temperature achieved in the static field study enables the effective mass deduced from the pulsed field experiment to be refined: $m^* = (4.9\text{--}5.8)m_0$ for the $T_c = 10$ K samples and $m^* \approx 5m_0$ for the $T_c = 26$ K sample. Analysis of the field dependence of the quantum oscillations leads to an estimate of the Dingle temperature $T_D \approx 6$ K, corresponding to a mean free path $\ell \approx 320$ Å.

Given that for a two-dimensional FS, the electronic specific heat (Sommerfeld coefficient) is $\gamma_{el} = (\pi N_A k_B^2 a^2 / 3\hbar^2) m^*$ (where k_B is the Boltzmann constant, N_A is Avogadro number, and $a = 3.86$ Å is the in-plane lattice constant), m^* deduced from quantum oscillations converts to $\gamma_{el} = 7.6 \pm 0.6 \text{ mJ mol}^{-1} \text{ K}^{-2}$ [41], in excellent agreement with that measured directly for overdoped polycrystalline $\text{Tl}_2\text{Ba}_2\text{CuO}_{6+\delta}$ ($7.0 \pm 2.0 \text{ mJ mol}^{-1} \text{ K}^{-2}$) [42]. The mass enhancement appears to be rather doping independent in this doping range, as expected from the relatively doping independent Sommerfeld coefficient [42] extracted from heat capacity measurements.

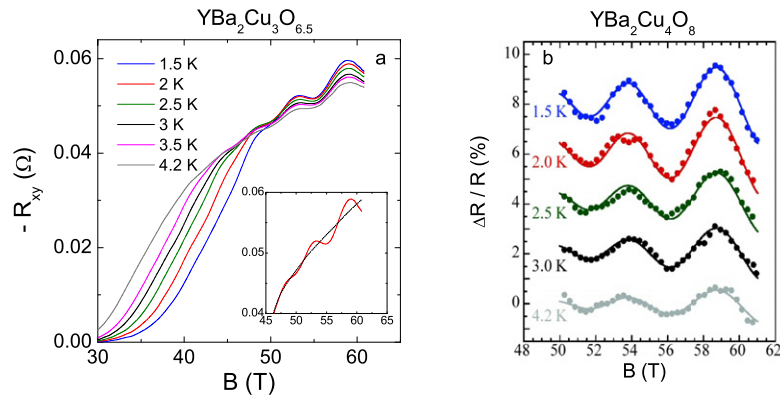


Fig. 3. (a) $-R_{xy}$ as a function of magnetic field B , for $\text{YBa}_2\text{Cu}_3\text{O}_{6.5}$, at different temperatures between 1.5 and 4.2 K (from [43]). The field is applied normal to the CuO_2 planes ($B \parallel c$) and the current is along the a -axis of the orthorhombic crystal structure ($I \parallel a$). Note that $R_{xy} < 0$. The inset shows a zoom on the data at $T = 2$ K, with a fitted monotonic background (dashed line). (b) The oscillatory component of the 4-point measurements of the magnetoresistance for $\text{YBa}_2\text{Cu}_4\text{O}_8$ at various temperatures. Solid lines are best fits to Eq. (1) giving $m^* = (2.7 \pm 0.3)m_0$ (from [44]).

We can thus make quantitative comparisons between quasiparticle properties derived from quantum oscillations at high fields and those measured directly by transport, ARPES and thermodynamics at zero field. This good overall consistency implies that the FS contains only one single quasi-two-dimensional (Q2D) sheet, as measured with quantum oscillations.

In summary, the FS of overdoped $\text{Tl}_2\text{Ba}_2\text{CuO}_{6+\delta}$ is characterized by a large Q2D Fermi cylinder covering $\sim 65\%$ of the first Brillouin zone. All the numbers deduced from these low temperature/high magnetic field studies are in excellent agreement with other experimental techniques (zero and low magnetic field) in the same material at similar doping levels. Despite strong electron–electron interactions, the observation of quantum oscillations implies that quasiparticles exist at all points of the FS of overdoped $\text{Tl}_2\text{Ba}_2\text{CuO}_{6+\delta}$. The observation of genuine quantum oscillations in $\text{Tl}_2\text{Ba}_2\text{CuO}_{6+\delta}$ supports the recognized idea that generalized Fermi-liquid theory can be applied on the overdoped side of the phase diagram, and that deviations from the Fermi–Dirac statistics are not relevant above 350 mK [41].

4. Early measurements of quantum oscillations in underdoped $\text{YBa}_2\text{Cu}_3\text{O}_y$ and $\text{YBa}_2\text{Cu}_4\text{O}_8$

The open issue is now to understand how the large FS enclosing $1 + p$ carriers for overdoped cuprates evolves as the system is driven closer to the Mott insulating phase. As shown by ARPES measurements for example, the underdoped regime is highly anomalous and the FS seems to consist of disconnected “Fermi arcs” [11]. The fundamental question that can be addressed with quantum oscillation measurements is whether underdoped copper oxides have a closed and coherent FS, and if so, whether it is topologically different from that seen in the overdoped regime.

Fig. 3a shows the first convincing evidence of quantum oscillations in the Hall resistance of $\text{YBa}_2\text{Cu}_3\text{O}_{6.5}$ ($T_c = 57.5$ K, $p = 0.10$) where oscillations are clearly seen above the resistive superconducting transition [43]. The inset of Fig. 3a shows the 2 K isotherm and a smooth background curve (dashed line). A subtraction of this monotonic background allows to show that the oscillations are periodic in $1/B$, as expected for oscillations that arise from Landau quantization. The Fourier transform consists in a single peak at $F = (530 \pm 20)$ T. Oscillations of the same frequency are also observed in R_{xx} , albeit with a smaller amplitude [45]. The temperature dependence of the amplitude of the oscillations allows to deduce the effective mass $m^* = (1.9 \pm 0.1)m_0$. The observation of genuine quantum oscillations has been confirmed by measurements of de Haas–van Alphen effect in $\text{YBa}_2\text{Cu}_3\text{O}_{6.5}$ [46] with the same frequency and effective mass. As a thermodynamic measurement, it firmly confirms the existence of well-defined quasiparticles at the FS with a substantial mean free path.

Fig. 3b shows the temperature dependence of the oscillatory component of the magnetoresistance for the related stoichiometric compound $\text{YBa}_2\text{Cu}_4\text{O}_8$ ($T_c = 82$ K, $p = 0.14$) between 50 and 61 T [44]. A fit of Eq. (1) to the data (shown by solid lines in Fig. 3b) gives a single frequency $F = (660 \pm 30)$ T, an effective mass $m^* = (2.7 \pm 0.3)m_0$ and an average SdH mean free path $\ell_{\text{SdH}} = (90 \pm 30)$ Å. Quantum oscillations in $\text{YBa}_2\text{Cu}_4\text{O}_8$ have also been observed using a tunnel-diode oscillator technique (TDO) in pulsed magnetic fields up to 85 T in Los Alamos [47]. The oscillation frequency, $F = (660 \pm 15)$ T, and the effective mass, $m^* = (3.1 \pm 0.3)m_0$, are consistent with the measurements in Toulouse.

We can thus conclude that underdoped cuprates have a closed and coherent Fermi surface, albeit with a much reduced size as compared to the overdoped ones (the frequency of oscillations being 30 times smaller), which has strong implications for the low temperature ground state, as will be discussed in Section 6.

4.1. Evidence for multiples frequencies in $\text{YBa}_2\text{Cu}_3\text{O}_y$

In order to get more insight on the Fermi surface of underdoped cuprates, we have performed high-precision measurements of the Shubnikov–de Haas effect in $\text{YBa}_2\text{Cu}_3\text{O}_{6.59}$ ($p = 0.108$) by measuring the c -axis magnetoresistance up to 80 T.

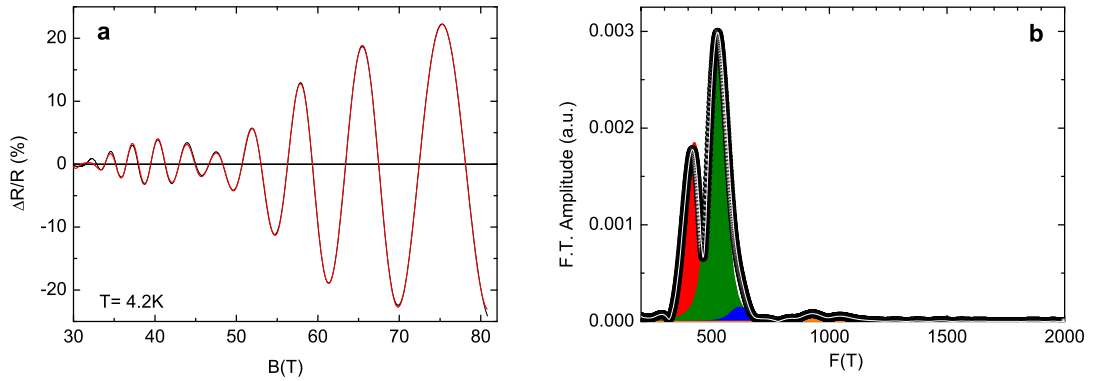


Fig. 4. (a) SdH oscillations of the c -axis magnetoresistance measured at 4.2 K in $\text{YBa}_2\text{Cu}_3\text{O}_{6.59}$ ($p = 0.108$) and up to 80 T as a function of magnetic field. A beating effect is clearly resolved, showing that the main oscillation is composed of three closely spaced frequencies. (b) The Fourier transform of the oscillatory signal (black line) can be decomposed into 3 closely spaced frequencies. (For interpretation of the references to colour in this figure, the reader is referred to the web version of this article.)

The greatly improved signal over noise ratio stems from the highly anisotropic nature of the cuprates. Indeed, the c -axis resistive signal can be two orders of magnitude higher than the in-plane resistive signal.

Fig. 4a shows the oscillatory component of the c -axis magnetoresistance of $\text{YBa}_2\text{Cu}_3\text{O}_{6.59}$ at $T = 4.2$ K up to 80 T. By measuring c -axis resistivity, this is the cyclotron motion of electrons in a plane perpendicular to the applied magnetic field which is being probed. The improved sensitivity of the measurements allows the discovery of some important details on the electronic structure of underdoped $\text{YBa}_2\text{Cu}_3\text{O}_y$. While the amplitude of the oscillations should grow exponentially with magnetic field for a single frequency, a modulation of the amplitude of the oscillations (beating effect) can be noticed in the raw data, which is the signature of the presence of more than one frequency in the oscillatory spectrum. In order to resolve the multiple frequencies, we have performed fits of Eq. (1) to the data with three frequencies. Fig. 4b shows a Fourier transform of the data (black circles) along with the relative amplitude of three frequencies used in the fit: a main frequency $F_1 = 521 \pm 15$ T (green peak) and two satellites: a high intensity one at $F_2 = 420 \pm 15$ T (red peak) and a weaker one at $F_3 = 619 \pm 40$ T (blue peak). The broad feature in the FT around 1000 T corresponds most likely to harmonics of F_1 and F_2 . A possible explanation for the multiple frequencies observed here is to invoke both a slight modulation of the FS sheet along the c -axis (warping) and a bilayer splitting effect, the latter being intrinsic to $\text{YBa}_2\text{Cu}_3\text{O}_y$ which contains two closely spaced CuO_2 planes.

In such a situation, angle dependent measurements are needed to clarify whether the multiple frequencies arise from a warped three-dimensional surface or from separate Fermi sheets. Indeed, if the multiple frequencies arise from the neck and belly orbits, they should follow an angle dependence given by Eq. (2). c -axis longitudinal magnetoresistance measurements in $\text{YBa}_2\text{Cu}_3\text{O}_{6.5}$ have been performed at different angles between the CuO_2 plane and the magnetic field (up to 57°).

Assuming that the frequency splitting is due to warping of the FS, fits of Eq. (2) for a quasi-2D FS have been performed to the entire set of data. A method based on a genetic algorithm that explores a wide parameter space for the entire data set allows to fit both the field and the angle dependence of the resistivity simultaneously and then iterating with fits to the field and temperature dependence [33]. The fitted model involves two warped surfaces ($F_{S1} = 478$ T and $F_{S2} = 526$ T), in agreement with the analysis presented above. Note that the weaker signal with a frequency near $F_3 = 630$ T has not been incorporated in the model because its intensity disappears as the angle is tilted away from the CuO_2 planes.

The closeness in size of the cylinders, in the Dingle temperatures, and in the cyclotron masses suggest that the two separate pieces of FS might be more closely related, as it is the case for example in a bilayer splitting scenario. In addition, these measurements uncover for the first time the effects of Zeeman splitting in the measurements [33], known as the spin-zero effect due to the interference of spin-up and spin-down contributions on each Fermi sheets. The spin zero effect manifests itself as a vanishing of the amplitude of the oscillations for the entire field range at a specific angle. This indicates that the interaction of the magnetic field with the spins of the electrons is a simple symmetric Zeeman splitting, linear in magnetic field, a key sign that the quasiparticles in the cuprates behave as free spins (i.e. there is no substantial magnetic order in the CuO_2 plane).

4.2. Doping dependence of the frequency of quantum oscillations in $\text{YBa}_2\text{Cu}_3\text{O}_y$

A doping evolution of the dominant frequency is of prime interest to settle the topology of the FS. The oscillatory parts of the magnetoresistance of $\text{YBa}_2\text{Cu}_3\text{O}_y$ at seven different doping levels ($0.098 < p < 0.126$) between 33 T and 81 T is shown in Fig. 5. The vertical dashed lines emphasize the doping evolution of the spectrum: as the doping level varies from $p = 0.098$ to $p = 0.126$ maxima are not in phase, indicating a frequency evolution in the spectrum as the system is doped. The signal becomes very small as the doping level departs from high quality oxygen ordered $\text{YBa}_2\text{Cu}_3\text{O}_y$ ortho-II ($p \approx 0.11$). We have therefore multiplied the oscillating signal by a factor for some doping levels, as indicated in Fig. 5a.

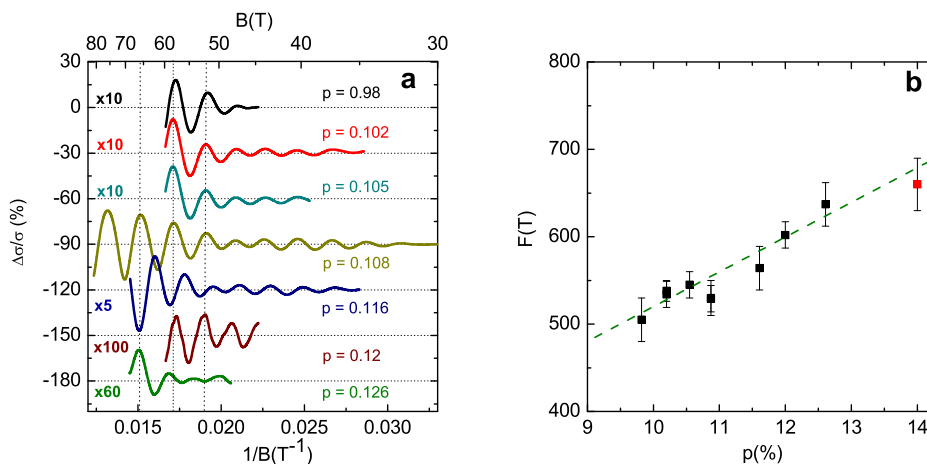


Fig. 5. (a) Oscillatory part of the *c*-axis magnetoresistance plotted as $1/B$ in $\text{YBa}_2\text{Cu}_3\text{O}_y$ for different doping levels p , with $0.098 \leq p \leq 0.126$ ($T = 4.2$ K for $p = 0.108$ and $T = 1.5$ K for the other doping levels). Note that the curves have been multiplied by a factor indicated in the figure and offset for clarity. A subtle change can be seen in the frequency as the doping level is increased. (b) The doping dependence of the frequency of quantum oscillations deduced from the Onsager relation applied to the raw data shown in (a). The red point at $p = 0.14$ corresponds to in-plane resistivity measurements in $\text{YBa}_2\text{Cu}_4\text{O}_8$ from Ref. [44]. (For interpretation of the references to colour in this figure legend, the reader is referred to the web version of this article.)

While there is a subtle change in the frequency of oscillations, a careful analysis by indexing the maximum of the oscillations versus $1/B$ (Onsager relation [28]) yields the doping dependence of the frequency shown in Fig. 5b. Even though this approach is not strictly valid in the case of multiple frequencies, simulations show that in the relevant range of parameters, the frequency extracted from the Onsager relation is close to the dominating frequency. There is a clear trend of increasing frequency as the doping increases, that is to say the size of the small Fermi pocket increases when the system is doped. This doping evolution is a key feature to discuss the topology of the FS in the underdoped regime and calls for a close theoretical investigation as no theory is currently able to explain this doping evolution.

5. The case for an electron pocket

5.1. Experimental evidence

The normal state Hall coefficient $R_H = tR_{xy}/B$, where t is the sample thickness, measured at high field is displayed in Fig. 6a as a function of temperature for overdoped $\text{Tl}_2\text{Ba}_2\text{CuO}_{6+\delta}$ [3] ($p \approx 0.25$, green symbols), underdoped $\text{YBa}_2\text{Cu}_3\text{O}_{6.5}$ ($p = 0.097$, red symbols) and $\text{YBa}_2\text{Cu}_3\text{O}_{6.67}$ ($p = 0.12$, blue line) [48]. In overdoped $\text{Tl}_2\text{Ba}_2\text{CuO}_{6+\delta}$, the Hall coefficient is almost temperature independent and is positive (e.g. hole-like). It extrapolates to a small number corresponding to a large carrier density ($R_H = 1/ne$). However, for underdoped $\text{YBa}_2\text{Cu}_3\text{O}_y$, $R_H(T)$ goes from positive at high temperature to negative as $T \rightarrow 0$. As demonstrated in Refs. [48,49], the negative R_H is shown to be unambiguously a property of the normal state. The most natural explanation for the negative R_H is the presence of an electron pocket in the FS. In a scenario in which the FS contains both electron and hole sheets, the sign of R_H depends on the relative magnitude of the electron and hole densities n_e and n_h and mobilities μ_e and μ_h ($\mu = e\tau/m^*$). The fact that $R_H < 0$ at low temperature implies that $\mu_e > \mu_h$ at low temperature. Given strong inelastic scattering, this inequality can then easily be inverted at high temperature, offering a straightforward mechanism for the sign change in R_H . The presence of an electron pocket in the FS of underdoped $\text{YBa}_2\text{Cu}_3\text{O}_y$ has been strengthened by the observation of negative Seebeck coefficients in underdoped $\text{YBa}_2\text{Cu}_3\text{O}_y$ as shown in Fig. 7a [50] and more thoroughly discussed in the next section.

In addition to the negative Hall and Seebeck coefficients at low temperature, another indication for the presence of an electron pocket in the FS of underdoped $\text{YBa}_2\text{Cu}_3\text{O}_y$ comes from the phase shift of about π between the quantum oscillations in the transverse magnetoresistance R_{xx} and in the Hall resistance R_{xy} [45], as shown in Fig. 6b. Indeed, it has been shown that for a 2D electron gas, the diagonal and off-diagonal elements of the resistivity tensor oscillate in anti-phase as a function of the magnetic field [51].

5.2. Lifshitz transition

The doping dependence of the frequency linked to the electron pocket in Fig. 5 shows that the size of pocket decreases as the doping decreases. Unfortunately, due to sample quality and the lack of oxygen ordering below $p = 0.10$, it has not yet been possible to detect quantum oscillations in $\text{YBa}_2\text{Cu}_3\text{O}_y$ below $p = 0.097$. In order to extract more information on the electron pocket at lower doping, it is instructive to discuss the doping dependence of the Hall and Seebeck coefficients. Fig. 7a shows subsequent measurements of the normal-state Seebeck coefficient, performed at the LNCMI-G up to 28 T as a function of temperature for several doping levels from $p = 0.08$ to $p = 0.12$ [52].

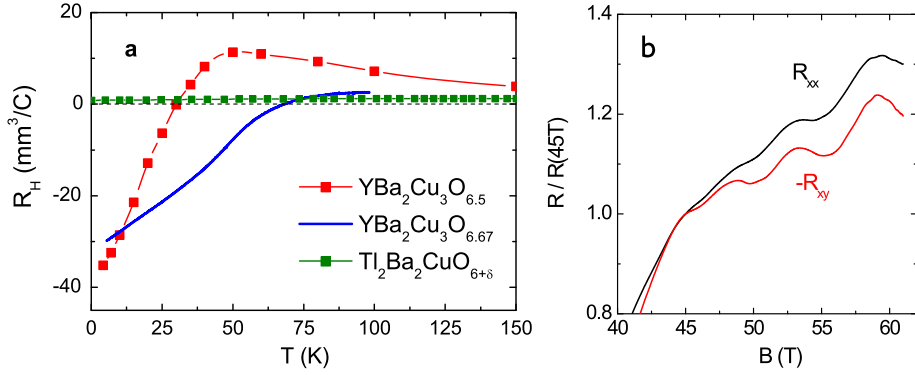


Fig. 6. (a) Hall coefficient R_H versus T for $\text{YBa}_2\text{Cu}_3\text{O}_{6.5}$ [48] (red symbols), $\text{YBa}_2\text{Cu}_3\text{O}_{6.67}$ [48] (blue line) and $\text{Tl}_2\text{Ba}_2\text{CuO}_{6+\delta}$ (green symbols) [3], at $B = 55$, 45 and 16 T, respectively. (b) π -Phase shift between the quantum oscillations measured in the transverse magnetoresistance R_{xx} and in the Hall resistance R_{xy} measured at $T = 1.5$ K, from [45]. Note the curves have been renormalized by their value at 45 T and the Hall resistance has been multiplied by -1 for clarity. (For interpretation of the references to colour in this figure legend, the reader is referred to the web version of this article.)

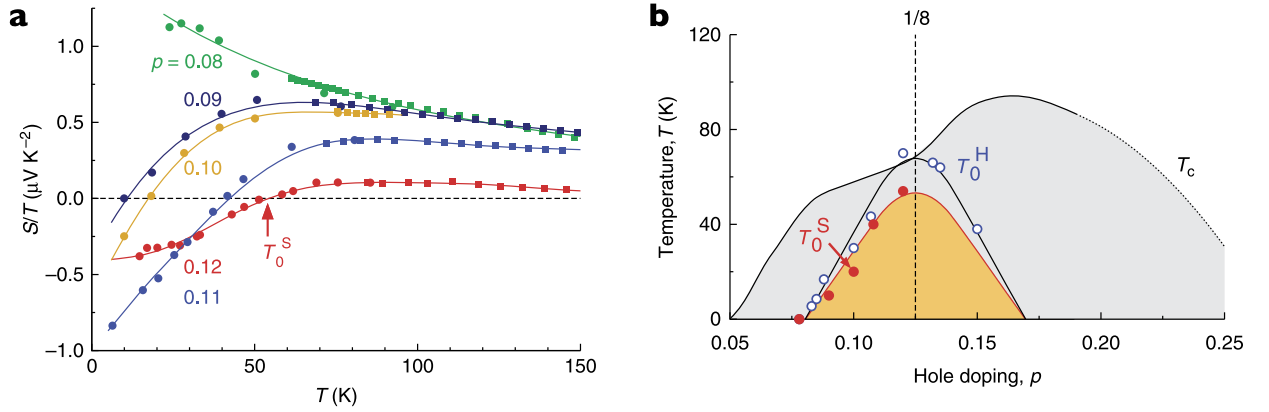


Fig. 7. (a) Seebeck coefficient of $\text{YBa}_2\text{Cu}_3\text{O}_y$ at five different doping levels p as indicated. The data have been taken at 28 T at the LNCMI Grenoble (from Ref. [52]). T_0^S marks the temperature at which the Seebeck coefficient changes sign as a function of temperature. (b) Phase diagram of $\text{YBa}_2\text{Cu}_3\text{O}_y$, showing the zero-field superconducting transition temperature T_c (black line) as a function of doping and the sign-change temperature T_0^H of R_H , and T_0^S are shown in open blue circles (from [49]) and red circles respectively. (For interpretation of the references to colour in this figure legend, the reader is referred to the web version of this article.)

When a temperature difference ΔT is applied along the x -axis of a metallic sample, a longitudinal voltage V_x develops across the sample, and the Seebeck coefficient (or thermopower) is defined as $S = V_x/\Delta T$. In a Boltzmann picture for a single band metal, the magnitude of this coefficient is given by: $S/T = \pm \frac{\pi^2}{2} \frac{k_B}{e} \frac{1}{T_F}$ where $T_F = (\hbar^2/2k_B)(k_F^2/m^*)$ is the Fermi temperature. The sign of S is controlled by the carrier type: positive for holes, negative for electrons. S/T for samples with $p > 0.08$ undergoes a change of sign, from positive at high temperature to negative at low temperature, similar to the sign change reported in the Hall coefficient R_H of underdoped $\text{YBa}_2\text{Cu}_3\text{O}_y$ [49]. The fact that both S and R_H are negative in the normal state at $T \rightarrow 0$ is compelling evidence for an electron-like sheet in the FS. Moreover, the Fermi pocket measured by quantum oscillations has a sufficiently small Fermi energy to account for the large magnitude of the negative thermopower at $T \rightarrow 0$ [50].

These measurements confirm the trend of $R_H(T)$ going from positive at high temperature to negative as $T \rightarrow 0$ for all doping levels for $p > 0.08$. For $p \leq 0.08$, $R_H(T)$ and $S(T)/T$ remain positive at all temperatures. Fig. 7b shows the phase diagram for $\text{YBa}_2\text{Cu}_3\text{O}_y$ (T_c line in black symbols) at which the characteristic temperatures T_0^H and T_0^S , where the Hall and Seebeck coefficients change sign, are plotted in open blue and red circles respectively [52]. We see that T_0^H and T_0^S both peak at $p = 1/8$ and below this maximum, T_0^H and T_0^S decrease monotonically (and linearly) to zero at $p = 0.08$. At this lowest doping, there is no sign change of R_H and S/T (see data for the $p = 0.08$ sample in Fig. 7a). This drastic change of behaviour in R_H and S/T points to a topological change in the FS of $\text{YBa}_2\text{Cu}_3\text{O}_y$ as the doping is decreased below a critical doping $p < p_L = 0.08$, either caused by a Lifshitz transition where the closed electron pocket disappears or by a phase transition [53]. The latter conclusion is supported by muon spin rotation experiments [54,55] and neutron diffraction measurements [56] in strongly underdoped $\text{YBa}_2\text{Cu}_3\text{O}_y$ ($p < 0.08$), which show static incommensurate magnetic order at low temperature.

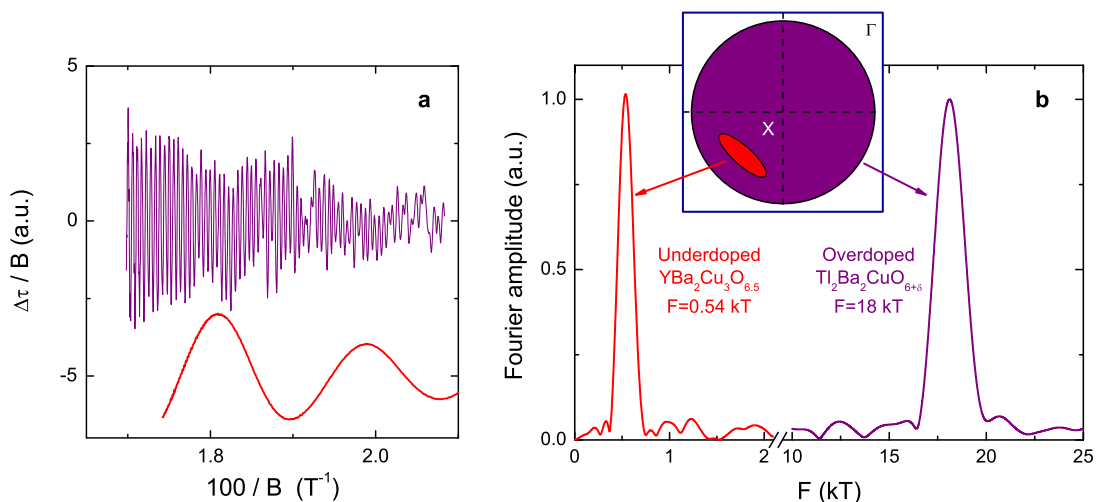


Fig. 8. (a) Oscillatory part of the magnetization (raw data) versus $1/B$ of $Tl_2Ba_2CuO_{6+\delta}$ (magenta) and $YBa_2Cu_3O_{6.5}$ (red). (b) Fourier analysis of the raw data shown in (a). The inset is a sketch of the size of the Fermi pocket in the first Brillouin zone deduced from the frequency of the quantum oscillations for $Tl_2Ba_2CuO_{6+\delta}$ (magenta) and $YBa_2Cu_3O_{6.5}$ (red). Note that the position in the Brillouin zone and the shape of the Fermi surfaces are arbitrary. (For interpretation of the references to colour in this figure legend, the reader is referred to the web version of this article.)

6. Comparison of quantum oscillations on both sides of the phase diagram

We now discuss the implications of quantum oscillations on both sides of the phase diagram of cuprates. In Fig. 8a, the oscillatory part of the magnetization for $YBa_2Cu_3O_{6.5}$ (red) and $Tl_2Ba_2CuO_{6+\delta}$ (magenta) are plotted together as $1/B$. There is a drastic difference in the frequency of the oscillations as shown by the corresponding Fourier transform in Fig. 8b. For overdoped $Tl_2Ba_2CuO_{6+\delta}$, a frequency $F = 18\,100$ T leads to an FS cross section area $A_F = 172.8\text{ nm}^{-2}$, which represents 65 % of the first Brillouin zone. Surprisingly, the frequency $F = 540$ T found for underdoped $YBa_2Cu_3O_{6.5}$ corresponds to an extremal area $A_F = 5.1\text{ nm}^{-2}$, which represents only 1.9 % of the first Brillouin zone. A sketch of the size of the pocket in the first Brillouin zone deduced from quantum oscillations is shown in the inset of Fig. 8b. Note that the position and shape of the Fermi surfaces are arbitrarily taken as this cannot be determined directly by quantum oscillation measurements. For $Tl_2Ba_2CuO_{6+\delta}$, a frequency $F = 18\,100$ T converts to a carrier density $n = 1.3 = 1 + p$ carrier per Cu atom, while for $YBa_2Cu_3O_{6.5}$, the frequency $F = 540$ T corresponds to $n = 0.038$ carrier per planar Cu atom.

The dramatic difference between the small pocket revealed by the low frequency reported for $YBa_2Cu_3O_{6.5}$ and the large cylindrical surface observed in overdoped $Tl_2Ba_2CuO_{6+\delta}$ reflects thus the difference in the carrier density on both side of the phase diagram. The measurements offer strong support for the scenario that below a critical doping level p_c ($0.14 < p_c < 0.27$) within the superconducting dome, cuprates undergo an FS reconstruction where the large hole-like FS reconstruct into small pockets. We will now show that the experimental findings in the underdoped regime are not compatible with band structure calculations and with doped Mott insulator scenarios.

6.1. Comparison with band structure calculations

Results obtained for overdoped $Tl_2Ba_2CuO_{6+\delta}$ are in excellent agreement with band structure calculations. For $YBa_2Cu_3O_{6.5}$, the FS deduced from band structure calculations consists of two large hole-like tubular CuO_2 sheets, plus three quasi-one-dimensional sheets. A subtle change in the Fermi energy can lead to the appearance of an additional small hole-like pocket [57], whose size may be comparable with the small pocket deduced from quantum oscillations. Few experimental observations rule out the FS derived from band structure calculations. If one assumes the small frequency corresponds to the small hole-like pocket at the Y point, it disagrees with the negative Hall effect (see Fig. 3a) which points to an electron pocket. Moreover, band structure calculations in $YBa_2Cu_4O_8$ have shown that the CuO/BaO band which gives rise to the small hole-like pocket at the Y point in $YBa_2Cu_3O_{6.5}$, is 400 meV below the Fermi energy, excluding that this band could give rise to a small pocket in $YBa_2Cu_4O_8$. We thus conclude that band structure calculations are incompatible with the measured quantum oscillations in both $YBa_2Cu_3O_{6.5}$ and $YBa_2Cu_4O_8$.

6.2. Four nodal hole pockets

A number of theories predict an FS made of four small hole-like pockets at nodal positions (carrier density equal to p) in the underdoped regime, going over to a large FS (carrier density equal to $1 + p$) when p exceeds a critical value p_c . Some of these are analogous to the usual spin-density-wave scenario in the sense that they invoke the onset of an ordered phase with broken symmetry below p_c [22,23,26,58,59], while others do not require any broken symmetry [60–62]. The second

class of scenarios predicts four-nodal hole pockets, whose area grows as the doping increases and merge into the large FS in the overdoped regime (see for example [60]). Assuming that ARPES detects only one side of a hole pocket at $(\pi/2, \pi/2)$, e.g. that the quasiparticle residue for the part of the pocket facing (π, π) is rather small, these scenarios could reconcile the quantum oscillations with photoemission measurements [22,63,64]. Assuming that the pocket is a hole pocket (of arbitrary curvature) and there is nothing else in the FS, and assuming also that n must be equal to the density of doped holes ($n = p = 0.1$ for $\text{YBa}_2\text{Cu}_3\text{O}_{6.5}$), the Luttinger sum rule is clearly violated, whether the relevant Brillouin zone includes one or two of these pockets (whether $n = n_{\text{SDH}} = 0.038$ or $n = 2 \times n_{\text{SDH}} = 0.076$). In addition, the negative Hall coefficient R_H at low temperature (see Fig. 3a) implies that the Shubnikov–de Haas frequency must come from a high-mobility electron pocket, because the amplitude of Shubnikov–de Haas oscillations depends exponentially on mobility μ , as $\exp(-\pi/\mu B)$. Therefore, a scenario based on a doped Mott insulator which predicts an FS made of four nodal hole-like pockets, is not compatible with our experimental findings.

6.3. Fermi surface reconstruction due to a competing order

The electron-like response of various transport quantities (see Section 5) combined with the small FS volume inferred from QO support the notion that the Fermi surface of underdoped $\text{YBa}_2\text{Cu}_3\text{O}_y$ (at least for $0.08 \leq p \leq 0.126$) and $\text{YBa}_2\text{Cu}_4\text{O}_8$ ($p = 0.14$) undergoes a reconstruction of the large FS predicted by band structure calculations. The standard mechanism for such a reconstruction is the onset of an ordered phase at $Q \neq 0$ that breaks the translational symmetry of the lattice. Several density wave instabilities have been proposed to account for this reconstruction: commensurate or incommensurate spin-density waves (SDW) [22,65] or d -density wave [26,66], stripe order (combination of SDW and charge-density wave (CDW) in the weak coupling limit [59,67]), 1D-CDW with strong nematicity of the large FS [68] and more recently biaxial CDW [69].

Each ordered phase leads to a specific FS, composed of a certain number of electron (and hole) sheets. Recent heat capacity measurements in $\text{YBa}_2\text{Cu}_3\text{O}_y$ ortho-II suggest that there is only one electron pocket per reduced Brillouin zone, and if sheets other than the observed electron pocket do exist, their associated quasiparticles should have a low effective mass [70]. Spin zero phenomena resulting from conventional Zeeman splitting (see Section 4.1) suggest that there is no spin order with a substantial component within the CuO_2 planes [33]. Finally, the comparative study of thermoelectric transport in underdoped $\text{YBa}_2\text{Cu}_3\text{O}_y$ and $\text{La}_{1.8-x}\text{Eu}_{0.2}\text{Sr}_x\text{CuO}_4$ (Eu-LSCO), a compound known to exhibit static stripe order, strongly supports the notion that CDW correlations are playing an important role in $\text{YBa}_2\text{Cu}_3\text{O}_y$ [52].

7. High field NMR measurements

7.1. Evidence for charge order

In order to detect the symmetry breaking suggested by transport measurements, NMR measurements of copper nuclei were performed in the conditions for which quantum oscillations are observed: same ultra pure, oxygen ordered, untwinned single crystals grown at the University of British Columbia, high magnetic fields applied along the c -axis, and low temperatures.

In general, the degeneracy of the nuclear energy levels is lifted by the interaction between the spin and the local magnetic field (via the Zeeman interaction). For a nucleus having a spin larger than $1/2$ (which is the case for ^{63}Cu) and being in a crystalline environment of symmetry lower than cubic, the energy levels are also affected by the interaction between the spin and the electric field gradient (via the electric quadrupole interaction). Through these two interactions, the NMR spectrum gives local, microscopic, information on the magnetic fields created by unpaired electrons and on the charge distribution due to the on-site electrons and the surrounding ions. Each NMR (central or satellite) line is a histogram of local magnetic fields and in addition, for the satellite lines, it is also a histogram of electric field gradients in the sample. A spatial modulation of the charge density will produce changes in the lineshapes which depend on the shape of the modulation. These changes potentially have a component in both the magnetic hyperfine shift (through modifications of the orbital susceptibility, of the spin susceptibility, and/or of the hyperfine coupling) and in the quadrupole frequency (through a modification of the electric field gradient tensor). In the simplest case, a bimodal distribution creates a line splitting. Any effect on the NMR lineshape can be considered as static on the typical timescale of an NMR spin-echo measurement of $10 \mu\text{s}$.

The major outcome of the NMR work [71] is the discovery of a line-splitting for those (so-called Cu2F) *planar* sites which lie below oxygen-filled chains (and the absence thereof for Cu2E sites below empty chains), as presented in Fig. 9. This splitting involves a differentiation of the quadrupole frequency (due to the interaction of the nucleus with electric field gradients) of Cu2F sites, therefore providing direct evidence for charge order in the CuO_2 planes. This splitting was actually resolved only for the ortho-II structure (doping $p \simeq 0.108$). The presence of charge order could be demonstrated for the ortho-VIII structure (doping $p = 0.12$) as well, but the splitting could not be directly observed there because of more complex Cu spectra. The evidence in this case comes from shoulders in the central line, due to modifications of hyperfine fields as observed also in ortho-II. This leaves more uncertainty regarding the actual charge pattern for ortho-VIII (see discussion below for ortho-II). More experiments (using ^{17}O NMR and/or other doping levels) are underway to clarify this question.

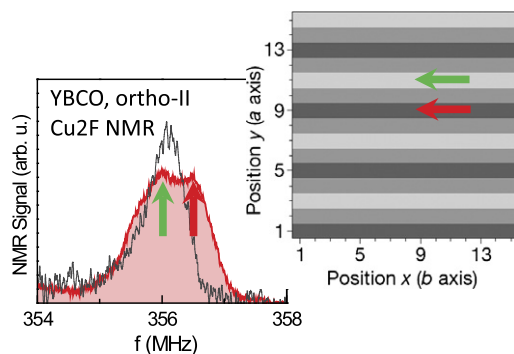


Fig. 9. Splitting of the high frequency quadrupole satellite of the Cu2F site (planar site below oxygen-filled chains) in $\text{YBa}_2\text{Cu}_3\text{O}_{6.54}$ ($p = 0.108$, ortho-II structure). This splitting has two components of equal magnitudes, one quadrupolar and one magnetic hyperfine. It is the quadrupolar component, related to the electric field gradient, which gives the direct evidence for charge order. The splitting occurs only for sufficiently high fields applied along the c -axis and for temperatures below 50 K, therefore providing a direct evidence that the charge order competes with superconductivity. The splitting is absent at Cu2E sites (or is too small to be resolved), which is direct evidence that the charge modulation has a one-dimensional nature. The simplest scenario is a stripe phase with a period of 4 lattice spacings. The two split Cu2F peaks correspond to lines with higher (dark grey) and lower (light grey) charge density, as indicated by the red and green arrows (see right panel). (For interpretation of the references to colour in this figure legend, the reader is referred to the web version of this article.)

7.2. Properties of the charge order

- *Charge order explains the Fermi surface reconstruction.* Not only must charge order reconstruct the Fermi surface (since it breaks translational symmetry), but the temperature onset T_{charge} for the charge order is also found to coincide with the drop and/or the sign change of the Hall and Seebeck coefficients. This demonstrates the direct link with the Fermi surface reconstruction.

- *The case for 4a-periodic charge-stripe order in ortho-II.* The absence of any resolved splitting at Cu2E sites in ortho-II imposes strong constraints on the pattern of charge order. A robust conclusion is that the charge modulation has a one-dimensional character though not necessarily purely 1D. The (first-order) description of the lineshape in terms of a simple splitting (rather than a more complex continuous shape) points towards a commensurate character of the modulation. There are actually only two main patterns which are consistent with these NMR constraints. We have argued that the physical context, particularly including the same phenomenology of the Hall and Seebeck coefficients between $\text{YBa}_2\text{Cu}_3\text{O}_y$ in high fields and in stripe ordered $\text{La}_{1.8-x}\text{Eu}_{0.2}\text{Sr}_x\text{CuO}_4$ in zero field [52], suggests that the charge pattern is the very same 4a-periodic charge-stripe order as observed in the La-214 family.

- *Absence of associated spin order.* A striking and unexpected aspect of the NMR results is the demonstration of the absence of spin-order associated with the charge order (at least in the investigated B, T range), in sharp contrast with the standard phenomenology of stripe materials. This definitely establishes that, in this region of the phase diagram, charge order is the leading order, of which spin order is a consequence.

- *Charge order is field-induced.* Another important aspect of the problem revealed by the NMR results, and which could not be addressed by transport measurements, is that the charge order is induced by the magnetic field (it is not observed at low fields). However, it only occurs for fields B perpendicular to the CuO_2 planes, not for fields within the planes. This means that it is not the strength of the field itself which causes the order but it is weakening of superconductivity by the field which, because of the electronic anisotropy, is much more efficient for $B \perp ab$ than for $B \parallel ab$. In other words, it is the occurrence of strong superconductivity which prevents charge order at low fields. The magnetic field effect shows that it makes no sense comparing the Fermi surface deduced from high field measurements with that deduced from zero-field measurements such as ARPES.

7.3. Consequences of the field-induced charge order

- It is likely that the charge-stripe order (at least in ortho-II) must be stabilized by the presence of a one-dimensional lattice potential from the chains in $\text{YBa}_2\text{Cu}_3\text{O}_y$, in the same manner as the low-temperature tetragonal distortion pins stripe order in La-214. Nevertheless, the occurrence of stripe order at the same electronic density $p \simeq 1/8$ in materials as different as $\text{La}_{2-x}\text{Ba}_x\text{CuO}_4$, Eu-LSCO and $\text{YBa}_2\text{Cu}_3\text{O}_y$ significantly strengthens the idea that there is a generic and intrinsic tendency towards charge order in CuO_2 planes, at least in this range of doping (evidence for a charge instability is also reported in underdoped $\text{Bi}_2\text{Sr}_2\text{CaCu}_2\text{O}_{8+\delta}$ [72]). Various indirect indications of charge and/or stripe order had already been reported in the literature, but the high-field NMR results in ortho-II are the first direct evidence on any cuprate other than La-214 which unambiguously shows stripe order.

- The striking effect of the magnetic field (in both magnitude and orientation) is one of the most clear-cut evidence to date of a description of underdoped cuprates in terms of competing orders, i.e. there is clearly here a competition between superconductivity and charge order. The closeness of the values of the transition temperatures T_{charge} and T_c is actually an indication that both orders have very close energies.

Very recently, X-ray experiments [73–75] have confirmed the presence of a charge-density wave instability in underdoped $\text{YBa}_2\text{Cu}_3\text{O}_y$ competing with superconductivity.

8. Perspectives

During these last 6 years, high magnetic field measurements have enabled a significant progress towards understanding the normal state properties of high- T_c cuprate superconductors. The observation of quantum oscillations (a key signature that quasiparticles with a substantial mean free path exist at low temperature) and the detection of the charge order responsible for the FS reconstruction are probably the two most striking examples. Nevertheless, a lot remains to be understood and a non-exhaustive list of hot questions includes:

- Is charge order a unidirectional $4a$ periodic stripe phase as NMR in $\text{YBa}_2\text{Cu}_3\text{O}_y$ ortho-II suggests or is it essentially a 2D incommensurate CDW as X-ray results for other doping level suggest? Can the two pictures be reconciled (for example are there additional, weaker, transverse modulations in ortho-II)?
- There are indications that strong charge correlations are already present in zero-field. Are there already static charge modulations in zero field? In that case, what is the nature of the high field state with respect to the zero-field state? A thermodynamic probe of the transitions in the (B, T) phase diagram would be highly desirable.
- How much of the (doping vs temperature) phase diagram of $\text{YBa}_2\text{Cu}_3\text{O}_y$ is affected by the charge order or by charge ordering tendencies? Is this tendency centred around $1/8$ doping, or does it decrease with doping like the pseudogap line? What is the relationship between charge order and the pseudogap?
- Uniaxial charge density wave can produce electron pocket if an electronic nematic state first develops. Biaxial charge density wave gives rise to electron pocket at the nodal position. The dimensionality of the charge order is thus crucial to understand the topology of the FS.
- How does the charge order in $\text{YBa}_2\text{Cu}_3\text{O}_y$ relate to the myriad of ordering phenomena reported in underdoped cuprates? In particular, is charge order ubiquitous?
- Do charge density wave fluctuations or correlations play a role in the mechanism of high- T_c superconductivity? The future seems to be bright for high magnetic field studies of high- T_c cuprates.

Acknowledgements

We wish to warmly thank our collaborators on transport studies of cuprates, in particular the group of Louis Taillefer at the University of Sherbrooke, the groups of N. Hussey and A. Carrington at the University of Bristol and more specifically our colleagues: A. Audouard, S. Badoux, A.F. Bangura, K. Behnia, C. Berthier, J.B. Bonnemaïson, J. Chang, R.A. Cooper, O. Cyr-Choinière, J. Day, R. Daou, N. Doiron-Leyraud, J.D. Fletcher, M.M.J. French, E. Hassinger, P.J. Heard, C. Jaudet, M. Horvatić, S. Krämer, F. Laliberté, D. LeBoeuf, S. Lepault, J. Levallois, A.P. Mackenzie, L. Malone, H. Mayaffre, M. Nardone, B.J. Ramshaw, M. Rondeau, M. Sutherland, T. Wu, A. Zitouni. The high quality single crystals of $\text{YBa}_2\text{Cu}_3\text{O}_y$ have been grown by the group of D. Bonn, W. Hardy and R. Liang from the University of British Columbia at Vancouver. Research support was provided by the French ANR projects DELICE and SUPERFIELD and Euromagnet II.

References

- [1] Cyril Proust, Etienne Boaknin, R.W. Hill, Louis Taillefer, A.P. Mackenzie, Phys. Rev. Lett. 89 (2002) 147003.
- [2] S. Nakamae, K. Behnia, N. Mangkorntong, M. Nohara, H. Takagi, S.J.C. Yates, N.E. Hussey, Phys. Rev. B 68 (2003) 100502.
- [3] A.P. Mackenzie, S.R. Julian, D.C. Sinclair, C.T. Lin, Phys. Rev. B 53 (1996) 5848.
- [4] T. Manako, Y. Kubo, Y. Shimakawa, Phys. Rev. B 46 (1992) 11019.
- [5] M. Abdel-Jawad, J.G. Analytis, L. Balicas, A. Carrington, J.P.H. Charmant, M.M.J. French, N.E. Hussey, Phys. Rev. Lett. 99 (2007) 107002.
- [6] R. Daou, N. Doiron-Leyraud, D. LeBoeuf, S.Y. Li, F. Laliberté, O. Cyr-Choinière, Y.J. Jo, L. Balicas, J.-Q. Yan, J.-S. Zhou, J.B. Goodenough, L. Taillefer, Nature Phys. 5 (2009) 31.
- [7] R.A. Cooper, Y. Wang, B. Vignolle, O.J. Lipscombe, S.M. Hayden, Y. Tanabe, T. Adachi, Y. Koiike, M. Nohara, H. Takagi, C. Proust, N.E. Hussey, Science 323 (2009) 603.
- [8] W.W. Warren, R.E. Walstedt, G.F. Brennert, R.J. Cava, R. Tycko, R.F. Bell, G. Dabbagh, Phys. Rev. Lett. 62 (1989) 1193.
- [9] H. Alloul, T. Ohno, P. Mendels, Phys. Rev. Lett. 63 (1989) 1700.
- [10] H. Yasuoka, T. Imai, T. Shimizu, in: Strong Correlation and Superconductivity, in: Springer Series in Solid State Sciences, vol. 89, 1989, p. 254.
- [11] M.R. Norman, H. Ding, M. Randeria, J.C. Campuzano, T. Yokoya, T. Takeuchi, T. Takahashi, T. Mochiku, K. Kadowaki, P. Guptasarma, D.G. Hinks, Nature 392 (1998) 157.
- [12] B. Fauqué, Y. Sidis, V. Hinkov, S. Pailhès, C.T. Lin, X. Chaud, P. Bourges, Phys. Rev. Lett. 96 (2006) 197001.
- [13] Y. Li, V. Balédent, N. Barisic, Y. Cho, B. Fauqué, Y. Sidis, G. Yu, X. Zhao, P. Bourges, M. Greven, Nature 455 (2008) 372.
- [14] S. De Almeida-Didry, Y. Sidis, V. Balédent, F. Giovannelli, I. Monot-Laffez, P. Bourges, Phys. Rev. B 86 (2012) 020504.
- [15] Jing Xia, Elizabeth Schemm, G. Deutscher, S.A. Kivelson, D.A. Bonn, W.N. Hardy, R. Liang, W. Siemons, G. Koster, M.M. Fejer, A. Kapitulnik, Phys. Rev. Lett. 100 (2008) 127002.
- [16] A. Shekhter, A. Migliori, J.B. Betts, F.F. Balakirev, R.D. McDonald, S.C. Riggs, B.J. Ramshaw, R. Liang, W.N. Hardy, D.A. Bonn, preprint, <http://arXiv.org/abs/1208.5810>, 2012.
- [17] R. Daou, J. Chang, D. LeBoeuf, O. Cyr-Choinière, F. Laliberté, N. Doiron-Leyraud, B.J. Ramshaw, R. Liang, D.A. Bonn, W.N. Hardy, L. Taillefer, Nature 463 (2010) 519.
- [18] M.J. Lawler, K. Fujita, J. Lee, A.R. Schmidt, Y. Kohsaka, C.K. Kim, H. Eisaki, S. Uchida, J.C. Davis, J.P. Sethna, E.-A. Kim, Nature 466 (2010) 347.
- [19] M.R. Norman, D. Pines, C. Kallin, Adv. Phys. 54 (2005) 715.
- [20] P.W. Anderson, Science 235 (1987) 1196.

- [21] V.J. Emery, S.A. Kivelson, *Nature* 374 (1995) 434.
- [22] A.V. Chubukov, D.K. Morr, *Phys. Rep.* 288 (1997) 355.
- [23] E.G. Moon, S. Sachdev, *Phys. Rev. B* 80 (2009) 035117.
- [24] S.A. Kivelson, I.P. Bindloss, E. Fradkin, V. Oganesyan, J.M. Tranquada, A. Kapitulnik, C. Howald, *Rev. Mod. Phys.* 75 (2003) 1201.
- [25] M. Vojta, *Adv. Phys.* 58 (2009) 699.
- [26] S. Chakravarty, R.B. Laughlin, D.K. Morr, C. Nayak, *Phys. Rev. B* 63 (2001) 094503.
- [27] C.M. Varma, *Phys. Rev. B* 55 (1997) 14554.
- [28] D. Shoenberg, *Magnetic Oscillations in Metals*, Cambridge Univ. Press, Cambridge, 1984.
- [29] W.J. de Haas, P.M. van Alphen, *Proc. Sect. Sci. K. Ned. Akad. Wet.* 33 (1930) 1106.
- [30] L. Shubnikov, W.Y. de Haas, *Comm. Phys. Lab. Univ. Leiden* (1930), 207a, 207c, 207d, 210a.
- [31] I.M. Lifshitz, A.M. Kosevich, *Zh. Eksp. Teor. Fiz.* 29 (1955) 730.
- [32] F.E. Richards, *Phys. Rev. B* 8 (1973) 2552.
- [33] B.J. Ramshaw, B. Vignolle, J. Day, R. Liang, W.N. Hardy, Cyril Proust, D.A. Bonn, *Nature Phys.* 7 (2011) 234.
- [34] P. Frings, J. Billette, J. Béard, O. Portugall, F. Lecouturier, G.L.J.A. Rikken, *IEEE Trans. Appl. Supercond.* 18 (2008) 592.
- [35] J. Béard, J. Billette, M. Suleiman, P. Frings, W. Knafo, G. Scheerer, F. Duc, D. Vignolles, M. Nardone, A. Zitouni, P. Delescluse, J.-M. Lagarrigue, F. Giquel, B. Griffe, N. Bruyant, J.-P. Nicolin, G.L.J.A. Rikken, R.B. Lyubovskii, G.V. Shilov, E.I. Zhilyaeva, R.N. Lyubovskaya, A. Audouard, *Eur. Phys. J. Appl. Phys.* 59 (2012) 30201.
- [36] N.E. Hussey, M. Abdel-Jawad, A. Carrington, A.P. Mackenzie, L. Balicas, *Nature* 425 (2003) 814.
- [37] M. Plate, J.D.F. Mottershead, I.S. Elfimov, D.C. Peets, Ruixing Liang, D.A. Bonn, W.N. Hardy, S. Chuzbaian, M. Falub, M. Shi, L. Patthey, A. Damascelli, *Phys. Rev. Lett.* 95 (2005) 077001.
- [38] D.J. Singh, W.E. Pickett, *Physica C* 203 (1992) 193.
- [39] B. Vignolle, A. Carrington, R.A. Cooper, M.M.J. French, A.P. Mackenzie, C. Jaudet, D. Vignolles, C. Proust, N.E. Hussey, *Nature* 455 (2008) 952.
- [40] A.F. Bangura, P.M.C. Rourke, T.M. Benseman, M. Matusiak, J.R. Cooper, N.E. Hussey, A. Carrington, *Phys. Rev. B* 82 (2010) 140501(R).
- [41] P.M.C. Rourke, A.F. Bangura, T.M. Benseman, M. Matusiak, J.R. Cooper, A. Carrington, N.E. Hussey, *New J. Phys.* 12 (2010) 105009.
- [42] J.W. Loram, K.A. Mirza, J.M. Wade, J.R. Cooper, W.Y. Liang, *Physica C* 235 (1994) 134.
- [43] Nicolas Doiron-Leyraud, Cyril Proust, David LeBoeuf, Julien Levallois, Jean-Baptiste Bonnemaïson, Ruixing Liang, D.A. Bonn, W.N. Hardy, Louis Taillefer, *Nature* 447 (2007) 565.
- [44] A.F. Bangura, J.D. Fletcher, A. Carrington, J. Levallois, M. Nardone, B. Vignolle, P.J. Heard, N. Doiron-Leyraud, D. LeBoeuf, L. Taillefer, S. Adachi, C. Proust, N.E. Hussey, *Phys. Rev. Lett.* 100 (2008) 047004.
- [45] C. Jaudet, J. Levallois, A. Audouard, D. Vignolles, B. Vignolle, R. Liang, D.A. Bonn, W.N. Hardy, N.E. Hussey, L. Taillefer, C. Proust, *Physica B* 404 (2009) 354.
- [46] Cyril Jaudet, David Vignolles, Alain Audouard, Julien Levallois, D. LeBoeuf, Nicolas Doiron-Leyraud, B. Vignolle, M. Nardone, A. Zitouni, Ruixing Liang, D.A. Bonn, W.N. Hardy, Louis Taillefer, Cyril Proust, *Phys. Rev. Lett.* 100 (2008) 187005.
- [47] E.A. Yelland, J. Singleton, C.H. Mielke, N. Harrison, F.F. Balakirev, B. Dabrowski, J.R. Cooper, *Phys. Rev. Lett.* 100 (2008) 047003.
- [48] D. LeBoeuf, N. Doiron-Leyraud, J. Levallois, R. Daou, J.-B. Bonnemaïson, N.E. Hussey, L. Balicas, B.J. Ramshaw, R. Liang, D.A. Bonn, W.N. Hardy, S. Adachi, C. Proust, L. Taillefer, *Nature* 450 (2007) 533.
- [49] David LeBoeuf, Nicolas Doiron-Leyraud, B. Vignolle, Mike Sutherland, B.J. Ramshaw, J. Levallois, R. Daou, Francis Laliberté, Olivier Cyr-Choinière, Johan Chang, Y.J. Jo, L. Balicas, Ruixing Liang, D.A. Bonn, W.N. Hardy, Cyril Proust, Louis Taillefer, *Phys. Rev. B* 83 (2011) 054506.
- [50] J. Chang, R. Daou, C. Proust, D. LeBoeuf, N. Doiron-Leyraud, F. Laliberté, B. Pingault, B.J. Ramshaw, R. Liang, D.A. Bonn, W.N. Hardy, H. Takagi, A.B. Antunes, I. Sheikin, K. Behnia, L. Taillefer, *Phys. Rev. Lett.* 104 (2010) 057005.
- [51] T. Ando, *J. Phys. Soc. Jpn.* 37 (1974) 1233.
- [52] F. Laliberté, J. Chang, N. Doiron-Leyraud, E. Hassinger, R. Daou, M. Rondeau, B.J. Ramshaw, R. Liang, D.A. Bonn, W.N. Hardy, S. Pyon, T. Takayama, H. Takagi, I. Sheikin, L. Malone, C. Proust, K. Behnia, Louis Taillefer, *Nat. Commun.* 2 (2011) 432.
- [53] S.E. Sebastian, N. Harrison, E. Palm, T.P. Murphy, C.H. Mielke, R. Liang, D.A. Bonn, W.N. Hardy, G.G. Lonzarich, *Proc. Natl. Acad. Sci. USA* 107 (2010) 6175.
- [54] S. Sanna, G. Allodi, G. Concas, A.D. Hillier, R. De Renzi, *Phys. Rev. Lett.* 93 (2004) 207001.
- [55] F. Coneri, S. Sanna, K. Zheng, J. Lord, R. De Renzi, *Phys. Rev. B* 81 (2010) 104507.
- [56] D. Haug, V. Hinkov, Y. Sidis, P. Bourges, N.B. Christensen, A. Ivanov, T. Keller, C.T. Lin, B. Keimer, *New J. Phys.* 12 (2010) 105006.
- [57] A. Carrington, E.A. Yelland, *Phys. Rev. B* 76 (2007) 140508.
- [58] Jie Lin, A.J. Millis, *Phys. Rev. B* 72 (2005) 214506.
- [59] A.J. Millis, M.R. Norman, *Phys. Rev. B* 76 (2007) 220503.
- [60] K.-Y. Yang, T.M. Rice, F.-C. Zhang, *Phys. Rev. B* 73 (2006) 174501.
- [61] P.A. Lee, *Rep. Prog. Phys.* 71 (2008) 012501.
- [62] T.D. Stanescu, G. Kotliar, *Phys. Rev. B* 74 (2006) 125110.
- [63] N. Harrison, R.D. McDonald, J. Singleton, *Phys. Rev. Lett.* 99 (2007) 206406.
- [64] S. Chakravarty, C. Nayak, S. Tewari, *Phys. Rev. B* 68 (2003) 100504.
- [65] S.E. Sebastian, N. Harrison, E. Palm, T.P. Murphy, C.H. Mielke, R. Liang, D.A. Bonn, W.N. Hardy, G.G. Lonzarich, *Nature* 454 (2008) 200.
- [66] S. Chakravarty, H.-Y. Kee, *Proc. Natl. Acad. Sci.* 105 (2008) 8835.
- [67] J. Lin, A.J. Millis, *Phys. Rev. B* 78 (2008) 115108.
- [68] H. Yao, D.-H. Lee, S.A. Kivelson, *Phys. Rev. B* 84 (2011) 012507.
- [69] S.E. Sebastian, N. Harrison, R. Liang, D.A. Bonn, W.N. Hardy, C.H. Mielke, G.G. Lonzarich, *Phys. Rev. Lett.* 108 (2012) 196403.
- [70] S.C. Riggs, O. Vafek, J.B. Kemper, J.B. Betts, A. Migliori, F.F. Balakirev, W.N. Hardy, R. Liang, D.A. Bonn, G.S. Boebinger, *Nature Phys.* 7 (2011) 332.
- [71] T. Wu, H. Mayaffre, S. Krämer, M. Horvatić, C. Berthier, W.N. Hardy, R. Liang, D.A. Bonn, M.-H. Julien, *Nature* 477 (2011) 191.
- [72] C.V. Parker, P. Aynajian, E.H. da Silva Neto, A. Pushp, S. Ono, J. Wen, Z. Xu, G. Gu, A. Yazdani, *Nature* 468 (2010) 677.
- [73] J. Chang, E. Blackburn, A.T. Holmes, N.B. Christensen, J. Larsen, J. Mesot, Ruixing Liang, D.A. Bonn, W.N. Hardy, A. Watenphul, M.v. Zimmermann, E.M. Forgan, S.M. Hayden, *Nature Phys.* 8 (2012) 871.
- [74] G. Ghiringhelli, M. Le Tacon, M. Minola, S. Blanco-Canosa, C. Mazzoli, N.B. Brookes, G.M. De Luca, A. Frano, D.G. Hawthorn, F. He, T. Loew, M. Moretti Sala, D.C. Peets, M. Salluzzo, E. Schierle, R. Sutarto, G.A. Sawatzky, E. Weschke, B. Keimer, L. Braicovich, *Science* 337 (2012) 821.
- [75] A.J. Achkar, R. Sutarto, X. Mao, F. He, A. Frano, S. Blanco-Canosa, M. Le Tacon, G. Ghiringhelli, L. Braicovich, M. Minola, M. Moretti Sala, C. Mazzoli, Ruixing Liang, D.A. Bonn, W.N. Hardy, B. Keimer, G.A. Sawatzky, D.G. Hawthorn, *Phys. Rev. Lett.* 109 (2012) 167001.